AIP | The Journal of Chemical Physics

Rotationally resolved photoelectron spectra in resonance enhanced multiphoton ionization of SiF

Kwanghsi Wang and V. McKoy

Citation: The Journal of Chemical Physics **97**, 5489 (1992); doi: 10.1063/1.463782
View online: http://dx.doi.org/10.1063/1.463782
View Table of Contents: http://scitation.aip.org/content/aip/journal/jcp/97/8?ver=pdfcov
Published by the AIP Publishing

Articles you may be interested in

Rotationally resolved photoelectron spectra in resonance enhanced multiphoton ionization of H2O via the C 1 B 1 Rydberg state
J. Chem. Phys. **97**, 3905 (1992); 10.1063/1.462929

Rotationally resolved photoelectron spectra in resonance enhanced multiphoton ionization of Rydberg states of NH
J. Chem. Phys. **97**, 211 (1992); 10.1063/1.463619

Rotationally resolved photoelectron spectra in resonance enhanced multiphoton ionization of HCl via the F 1Δ2 Rydberg state
J. Chem. Phys. **95**, 8718 (1991); 10.1063/1.461256

Rotationally resolved photoelectron angular distributions in resonance enhanced multiphoton ionization of NO
J. Chem. Phys. **91**, 2235 (1989); 10.1063/1.457031

Rotational branching ratios at low photoelectron energies in resonant enhanced multiphoton ionization of NO
J. Chem. Phys. **90**, 2570 (1989); 10.1063/1.455953

This article is copyrighted as indicated in the article. Reuse of AIP content is subject to the terms at: http://scitation.aip.org/termsconditions. Downloaded to IP: 131.215.248.200 On: Sat, 17 Oct 2015 05:28:26

Rotationally resolved photoelectron spectra in resonance enhanced multiphoton ionization of SiF

Kwanghsi Wang and V. McKoy
Arthur Amos Noyes Laboratory of Chemical Physics,[a] California Institute of Technology, Pasadena, California 91125

(Received 9 June 1992; accepted 6 July 1992)

Results of calculations of rotationally resolved photoelectron spectra for resonance enhanced multiphoton ionization (REMPI) of SiF via the $B\,^2\Sigma^+$ $(4s\sigma)$, $C''\,^2\Sigma^+$ $(4p\sigma)$, and $C'\,^2\Pi$ $(4p\pi)$ Rydberg states are reported. In addition to the expected ΔN=even peaks, unusually strong $\Delta N=\pm 1$ transitions are predicted for photoionization of the $B\,^2\Sigma^+$ state. These unusual transitions are due to even angular momentum components of the photoelectron matrix element and arise from the formation of Cooper minima in the ionization channels and strong l mixing in the electronic continuum induced by the nonspherical molecular ion potential. Unexpected $\Delta N=0,\pm 2$ transitions, due to odd wave contributions to the photoelectron matrix element, are also predicted for photoionization of the $C''\,^2\Sigma^+$ state. Asymmetrical ion distributions with respect to $\Delta N=0$ are also predicted for the $C'\,^2\Pi$ state. Cooper minima are predicted to occur in the $l=2$ wave of the $k\pi$ photoelectron channel for the B state and in the $l=4$ wave of the $k\sigma$ and $k\pi$ channels for the C'' state. Photoelectron angular distributions provide further insight into the photoionization dynamics.

I. INTRODUCTION

SiF is an important intermediate radical in the etching of silicon by fluorinated gases in semiconductor fabrication.[1,2] Resonance enhanced multiphoton ionization (REMPI)[3] via the $C''\,^2\Sigma^+$ $(4p\sigma)$ and $C'\,^2\Pi$ $(4p\pi)$ Rydberg states of SiF have been shown to be a useful diagnostic tool for detection of SiF radicals resulting from surface reactions associated with these etching processes.[4,5] Since these ion signals were not rotationally resolved, the associated electronic structure and photoionization dynamics were not well explored. Studies of rotationally resolved REMPI ion spectra could clearly be helpful in the use of this technique as a diagnostic tool for detection of SiF radicals in etching plasmas.

In this paper, calculated rotationally resolved photoelectron spectra for one-color REMPI of SiF via the $B\,^2\Sigma^+$ $(4s\sigma)$, $C''\,^2\Sigma^+$ $(4p\sigma)$, and $C'\,^2\Pi$ $(4p\pi)$ Rydberg states are reported. The resulting spectra and underlying photoionization dynamics are illustrated and compared with the photoelectron spectra measured by Viswanathan *et al.*[6] in one-color REMPI of NO via the $A\,^2\Sigma^+$ $(3s\sigma)$, $D\,^2\Sigma^+$ $(3p\sigma)$, and $C\,^2\Pi$ $(3p\pi)$ states. An unusual $\Delta N=N^+-N'=0$ peak was observed in the ion spectra for (2+1) REMPI via the D $(3p\sigma)$ state of NO (Ref. 6). Here N^+ and N' are the rotational quantum numbers of the ionic and intermediate states exclusive of spin, respectively. This $\Delta N=0$ peak has been subsequently interpreted as arising from strong l mixing and the presence of Cooper minima in the ionization continua.[7] A Cooper minimum was also predicted to occur in photoionization of the C $(3p\pi)$ state but not in the A $(3s\sigma)$ state of NO. In this paper Cooper minima are predicted to occur in photoionization of the B $(4s\sigma)$ and C'' $(4p\sigma)$ states but not in the C' $(4p\pi)$ state of SiF. The role played by these Cooper minima in the ion rotational spectra is also discussed.

Here we choose the same REMPI processes and rotational branches used by Viswanathan *et al.*[6] in their studies of the A, D, and C states of NO. These are (1+1) REMPI via the $R_{22}(21.5)$ rotational branch of the $B\,^2\Sigma^+$ $(4s\sigma)$ state of SiF, (2+1) REMPI via the $S_{21}(11.5)$ rotational branch of the $C''\,^2\Sigma^+$ $(4p\sigma)$ state of SiF, and (2+1) REMPI via the $Q_{21}(13.5)$ rotational branch of the $C'\,^2\Pi$ $(4p\pi)$ state of SiF. Angle-integrated photoionization cross sections are reported along with photoelectron spectra for the laser polarized parallel and perpendicular to the flight direction of the photoelectron. To provide further insight into the photoionization dynamics, we also present photoelectron angular distributions.

II. THEORY AND CALCULATIONAL DETAILS

A. Differential cross section

The REMPI processes via the $B\,^2\Sigma^+$ $(4s\sigma)$, $C''\,^2\Sigma^+$ $(4p\sigma)$, and $C'\,^2\Pi$ $(4p\pi)$ Rydberg states of SiF can be summarized as follows:

$$\mathrm{SiF}[X\,^2\Pi(v_0, J_0)] \xrightarrow{\omega} \mathrm{SiF}^*[B\,^2\Sigma^+(v=0, J, N)] \xrightarrow{\omega} \mathrm{SiF}^+[X\,^1\Sigma^+(v^+, J^+=N^+)], \quad (1a)$$

$$\mathrm{SiF}[X\,^2\Pi(v_0, J_0)] \xrightarrow{2\omega} \mathrm{SiF}^*[C''\,^2\Sigma^+(v=0, J, N)] \xrightarrow{\omega} \mathrm{SiF}^+[X\,^1\Sigma^+(v^+, J^+=N^+)], \quad (1b)$$

and

$$\mathrm{SiF}[X\,^2\Pi(v_0, J_0)] \xrightarrow{2\omega} \mathrm{SiF}^*[C'\,^2\Pi(v=0, J, N)] \xrightarrow{\omega} \mathrm{SiF}^+[X\,^1\Sigma^+(v^+, J^+=N^+)]. \quad (1c)$$

[a]Contribution No. 8650.

This article is copyrighted as indicated in the article. Reuse of AIP content is subject to the terms at: http://scitation.aip.org/termsconditions. Downloaded to IP:

 0021-9606/92/205489-08$06.00 © 1992 American Institute of Physics

For linearly polarized light, ionization originating from each of the $(2J_0+1)$ magnetic sublevels of the initial state forms an independent channel under collision-free conditions. The rotationally resolved differential cross sections for ionization out of a J rotational level of the resonant intermediate state can be expressed in terms of Legendre polynomials as

$$\frac{d\sigma}{d\Omega} \propto \sum_{M_J M_{J^+}} \rho_{M_J M_J} |\Gamma_{M_J M_{J^+}}|^2$$

$$= \frac{\sigma}{4\pi}\left[1+\sum_{L=1}^{L_{\max}} \beta_{2L} P_{2L}(\cos\theta)\right], \tag{2}$$

where σ is the total cross section, β_{2L} the asymmetry parameters, θ the angle between the photoelectron and the polarization vector of the laser, $P_{2L}(\cos\theta)$ the Legendre polynomials, and $L_{\max}=2$ for the B state and 3 for the C'' and C' states. In Eq. (2), $\rho_{M_J M_J}$ is the population of a particular M_J level of the intermediate state created by n-photon resonant excitation. For rotational branches other than Q branches, $\rho_{M_J M_J}$ is a product of a 3-j symbol and a rotational line strength B,[8]

$$\rho_{M_J M_J} = \mathcal{N}\begin{pmatrix} J & n & J_0 \\ -M_J & 0 & M_J \end{pmatrix}^2 B, \tag{3}$$

where $\mathcal{N}$ is a normalization constant and $n=1$ for the B state and 2 for the C'' state. The rotational line strength B for single and multiphoton ($n=2$ and 3) excitation of diatomic molecules has been given by Earls[9] and Halpern *et al.*,[8] respectively. On the other hand, $\rho_{M_J M_J}$ becomes

$$\rho_{M_J M_J} = \mathcal{N}\left|\begin{pmatrix} J & 2 & J_0 \\ -M_J & 0 & M_J \end{pmatrix} B_2 + B_0\right|^2, \tag{4}$$

for Q branches.[10] Note that B_0 contains no polarization information but is crucial in determining the population $\rho_{M_J M_J}$ of the intermediate state for $(2+1)$ REMPI via the Q rotational branches. The evaluation of the B_0 and B_2 factors requires a summation over all possible paths and dipole-allowed virtual states in the two-photon excitation step. $|\Gamma_{M_J M_{J^+}}|^2$ of Eq. (2) is the probability for photoionization of a M_J level of the intermediate state leading to a M_{J^+} level of the ionic state. An expression for $\Gamma_{M_J M_{J^+}}$ within Hund's case (b) coupling scheme, which is suitable for the $B\,^2\Sigma^+$ and $C''\,^2\Sigma^+$ states, has been given by Dixit and McKoy.[11] However, the $C'\,^2\Pi$ state with its spin–orbit splitting constant $A=16.54\ \mathrm{cm}^{-1}$ and rotational constant $B_e=0.6363\ \mathrm{cm}^{-1}$ is best described by an intermediate coupling scheme between Hund's cases (a) and (b).[12] The expression for $\Gamma_{M_J M_{J^+}}$ with an intermediate coupling scheme between Hund's cases (a) and (b) has been recently given by Wang and McKoy.[13] The photoelectron signal detected along the polarization direction of the laser is given by $\beta_0+\beta_2+\beta_4+\beta_6$ and the perpendicular signal by $\beta_0-\frac{1}{2}\beta_2+\frac{3}{8}\beta_4-\frac{5}{16}\beta_6$ with $\beta_6=0$ for a $(1+1)$ REMPI process.

Parity selection rules[11,13–15] govern changes of rotational angular momentum upon photoionization. In the Hund's case (b) limit, they have been previously derived and are of the form[11,13–15]

$$\Delta N + l + \Delta p + \Delta q = \text{odd}, \tag{5}$$

where $\Delta p = p^+ - p$, $\Delta q = q^+ - q$. In Eq. (5), l is a partial wave component of the photoelectron, p the parity index[16] (0 for e states and 1 for f states), and q the index for Σ^- symmetry.[13] For $\Sigma^+ \rightarrow \Sigma^+$ transitions, Eq. (5) reduces to $\Delta N + l = \text{odd}$. For a Hund's case (a) basis, parity selection rules have the form

$$\Delta J + \Delta S + \Delta p + \Delta q + l = \text{even}, \tag{6}$$

where $\Delta J = J^+ - J$ and $\Delta S = S^+ - S$. In Eq. (6), J denotes the total angular momentum and S the total spin.

B. Numerical details

The wave functions for the $B\,^2\Sigma^+$ $(4s\sigma)$ state with electron configuration (core)9σ [(core) $=1\sigma^2\cdots 7\sigma^2 1\pi^4 2\pi^4$], the $C''\,^2\Sigma^+$ $(4p\sigma)$ state with configuration (core)10σ, and the $C'\,^2\Pi$ $(4p\pi)$ state with configuration (core)4π were obtained using the improved virtual orbital (IVO) method[17] with a fully relaxed core for the $X\,^1\Sigma^+$ ion. Note here and below that we use the molecular orbital $(9\sigma,10\sigma,4\pi)$ and united-atom $(4s\sigma,4p\sigma,4p\pi)$ designations interchangeably. The orbital basis used in these calculations consists of a $[6s,5p]$ contraction of the $(12s,9p)$ primitive Cartesian Gaussian basis of McLean and Chandler[18] augmented with two d functions ($\alpha=0.825$ and 0.275) on the silicon atom. On the fluorine we use a $[5s,4p]$ contraction of the $(10s,6p)$ uncontracted Cartesian Gaussian basis of Dunning[19] augmented with one s ($\alpha=0.095$), one p ($\alpha=0.075$), and two d ($\alpha=0.85$ and 0.15) functions. This basis is further augmented with five s ($\alpha=0.045$, 0.012, 0.004, 0.0015, and 0.0005), five p ($\alpha=0.035$, 0.010, 0.0036, 0.0012, and 0.0005), and three d ($\alpha=0.055$, 0.015, and 0.0025) functions on the center of mass (CM). With this basis and choice of wave functions, we obtain a total energy of $-387.259\,769$ a.u. for the $B\,^2\Sigma^+$ state at the equilibrium internuclear distance of $R_e=2.973\ a_0$.[12] The total energy is $-387.216\,978$ a.u. for the $C''\,^2\Sigma^+$ state at $R_e=2.884\ a_0$ and $-387.230\,866$ a.u. for the $C'\,^2\Pi$ state at $R_e=2.891\ a_0$.[12] The more penetrating $4s\sigma$ orbital of the $B\,^2\Sigma^+$ state and the $4p\sigma$ orbital of the $C''\,^2\Sigma^+$ state show a slow evolution with internuclear distance. For example, the single-center expansion of the $4s\sigma$ (9σ) orbital of the $B\,^2\Sigma^+$ state around the center of mass has the following partial wave compositions: 60.3% s, 35.5% p, 3.8% d, and 0.2% f at $R=2.2\ a_0$; 79.4% s, 18.9% p, 1.1% d, and 0.2% f at $R_e=2.973\ a_0$; and 81.5% s, 14.7% p, 3.2% d, and 0.3% f at $R=3.3\ a_0$. The angular momentum composition of the $4p\sigma$ (10σ) orbital of the $C''\,^2\Sigma^+$ state is 14.3% s, 51.1% p, 33.9% d, and 0.7% f at $R=2.2\ a_0$; 16.4% s, 71.6% p, 9.9% d, and 2.0% f at $R_e=2.884\ a_0$; and 11.2% s, 76.6% p, 9.5% d, and 2.4% f at $R=3.3\ a_0$. On the other hand, the composition of the $4p\pi$ (4π) orbital of the $C'\,^2\Pi$ state varies only slightly with internuclear distance. The $4p\pi$ orbital of the $C'\,^2\Pi$ state has 95.2% p, 4.3% d, and 0.2% f character at $R_e=2.891\ a_0$.

This article is copyrighted as indicated in the article. Reuse of AIP content is subject to the terms at: http://scitation.aip.org/termsconditions. Downloaded to IP: 131.215.248.200 On: Sat, 17 Oct 2015 05:28:26

TABLE I. Basis sets used in the separable potential of Eq. (7).

Symmetry	Center	Type of Gaussian function[a]	Exponents
σ	Si	Cartesian s	8.0, 4.0, 2.0, 1.0, 0.5, 0.2
		z	2.5, 1.0, 0.5, 0.2
	F	Cartesian s	8.0, 4.0, 2.0, 1.0, 0.5, 0.2
		z	2.5, 1.0, 0.5, 0.2
	CM	Spherical ($l=0-3$)	(a) 0.75, 0.25
			(b) 1.5, 0.75
			(c) 1.0, 0.5
π	Si	Cartesian x	8.0, 4.0, 2.0, 1.0, 0.5, 0.2
		xz	2.5, 1.0, 0.5, 0.2
	F	Cartesian x	8.0, 4.0, 1.0, 0.5, 0.2
		xz	2.5, 1.0, 0.5, 0.2
	CM	Spherical ($l=1-3$)	(a) 0.75, 0.25
			(b) 1.5, 0.75
			(c) 1.0, 0.5
δ	Si	Cartesian xy	8.0, 4.0, 2.0, 1.0, 0.5, 0.25, 0.1
	F	Cartesian xy	8.0, 4.0, 2.0, 1.0, 0.5, 0.25, 0.1
	CM	Spherical ($l=2-4$)	1.0, 0.5

[a]Cartesian Gaussian basis functions are defined as $\phi^{\alpha,l,m,n,A}(\mathbf{r})=\mathcal{N}(x-A_x)^l(y-A_y)^m(z-A_z)^n\exp(-\alpha|\mathbf{r}-\mathbf{A}|^2)$ and spherical Gaussian functions as $\phi^{\alpha,l,m,A}(\mathbf{r})=\mathcal{N}|\mathbf{r}-\mathbf{A}|^l\exp(-\alpha|\mathbf{r}-\mathbf{A}|^2)Y_{lm}(\Omega_{r-A})$, with $\mathcal{N}$ the normalization constant. (a), (b), and (c) are used for the $B\,^2\Sigma^+$, $C''\,^2\Sigma^+$, and $C'\,^2\Pi$ states, respectively.

To obtain the photoelectron orbitals we have used an iterative procedure, based on the Schwinger variational principle,[20,21] to solve the Lippmann–Schwinger equation. In this procedure, the static-exchange potential is approximated by

$$U(\mathbf{r},\mathbf{r}')=\sum_{ij}\langle\mathbf{r}|U|\alpha_i\rangle(U^{-1})_{ij}\langle\alpha_j|U|\mathbf{r}'\rangle, \tag{7}$$

where the matrix U^{-1} is the inverse of the matrix with elements $U_{ij}=\langle\alpha_i|U|\alpha_j\rangle$ and the α's are the discrete basis functions such as Cartesian or spherical Gaussian functions. U is twice the static-exchange potential with the long-range Coulomb potential removed. The basis sets used in the separable expansion of Eq. (7) are listed in Table I. The Lippmann–Schwinger equation with this separable potential $U(\mathbf{r},\mathbf{r}')$ can be readily solved and provides approximate photoelectron orbitals $\phi_k^{(0)}$. These solutions can be iteratively improved to yield converged photoelectron orbitals ϕ_k to the Lippmann–Schwinger equation containing the full static-exchange potential. In these studies, four iterations provided converged results.

All matrix elements arising in the solution of the Lippmann–Schwinger equation were evaluated by using single-center expansions about the center of mass. For converged results, the following parameters were used:[20,21]

(i) maximum partial wave expansion of the photoelectron continuum orbital=9;

(ii) maximum partial wave expansion of bound orbitals in the direct potential=80;

(iii) maximum partial wave expansion of the 1σ, 2σ, 3σ, 4σ, 5σ, 6σ, 7σ, 9σ, 10σ, 1π, 2π, and 4π bound orbitals in the exchange potential=40, 40, 35, 35, 35, 35, 35, 35, 35, 40, 35, and 35, respectively;

(iv) maximum partial wave expansion of $1/r_{12}$ in the direct and exchange terms=80 and 40, respectively;

(v) maximum partial wave expansion of the nuclear potential=80.

The radial integration grid extended to 64 a.u. and contained 800 points. The integration step sizes ranged from 0.01 to 0.16 a.u. up to 16 a.u. and up to 0.16 a.u. beyond this point.

III. RESULTS AND DISCUSSION

A. (1+1) REMPI via the $B\,^2\Sigma^+$ Rydberg state

To understand the underlying photoionization dynamics of rotationally resolved photoelectron spectra, it is useful to examine the angular momentum composition of the photoelectron matrix element. Figure 1 shows the magnitude of the (incoming-wave normalized) partial wave dipole amplitude $|D_l^{(-)}|$ as a function of photoelectron kinetic energy for the photoionization channels $4s\sigma\to k\sigma$ [Fig. 1(a)] and $4s\sigma\to k\pi$ [Fig. 1(b)] for the $B\,^2\Sigma^+$ $(4s\sigma)$ Rydberg state of SiF. A Cooper minimum, which is manifested by a change in the sign of the $l=2$ (d wave) component around the minimum in $|D_l^{(-)}|$, is clearly seen at a kinetic energy around 2.8 eV in the $k\pi$ channel. The actual sign change in the dipole matrix elements is seen in the principal-value (standing-wave normalized) dipole amplitude D_l^P (Refs. 20–22), as shown in the inset of Fig. 1(b) for the $l=2$ wave. The energy position of the minimum in $|D_l^{(-)}|$ differs somewhat from that of Cooper zero in D_l^P. This shift is due to l mixing in the electronic continuum and its influence on the renormalization of D_l^P to $D_l^{(-)}$. Similar behavior has also been predicted for (2+1) REMPI via the $f\,^1\Pi$ $(3p\sigma)$, $g\,^1\Delta$ $(3p\pi)$, and $h\,^1\Sigma^+$ $(3p\pi)$ Rydberg states of NH (Ref. 23). Minima are also seen in the $l=1$ and 3 components of $|D_l^{(-)}|$ near threshold for the $k\pi$ channel. However, the corresponding D_l^P do not show distinct sign changes (not shown).

Figure 1 also shows unexpectedly strong even angular momentum components in the photoelectron matrix elements for both the $k\sigma$ and $k\pi$ channels. Since the $4s\sigma$ orbital has strong s (79%) character, a dominant p wave component would be expected on the basis of an atomiclike picture. Although the $4s\sigma$ orbital of the B state has about 19% p character, which contributes to the even partial waves of the photoelectron, these large even-wave contributions arise primarily from strong angular momentum mixing in the electronic continuum brought about by the nonspherical molecular ion potential. Note that the SiF^+ core has a large dipole moment of 3.39 D, with respect to the center of mass.[24]

Figure 2 shows the rotationally resolved photoelectron spectra for (1+1) REMPI of the $B\,^2\Sigma^+$ $(4s\sigma)$ Rydberg state via the $R_{22}(21.5)$ rotational branch along with the photoelectron angular distributions [Fig. 2(d)]. The spectra for photoelectron detection parallel and perpendicular to the polarization vector of the radiation are shown in Figs. 2(b) and 2(c), respectively, for comparison with those for photoionization of the $A\,^2\Sigma^+$ $(3s\sigma)$ state of NO (Ref. 6). The alignment of the resonant $B\,^2\Sigma^+$ $(v=0,N$

This article is copyrighted as indicated in the article. Reuse of AIP content is subject to the terms at: http://scitation.aip.org/termsconditions. Downloaded to IP: 131.215.248.200 On: Sat, 17 Oct 2015 03:28:20

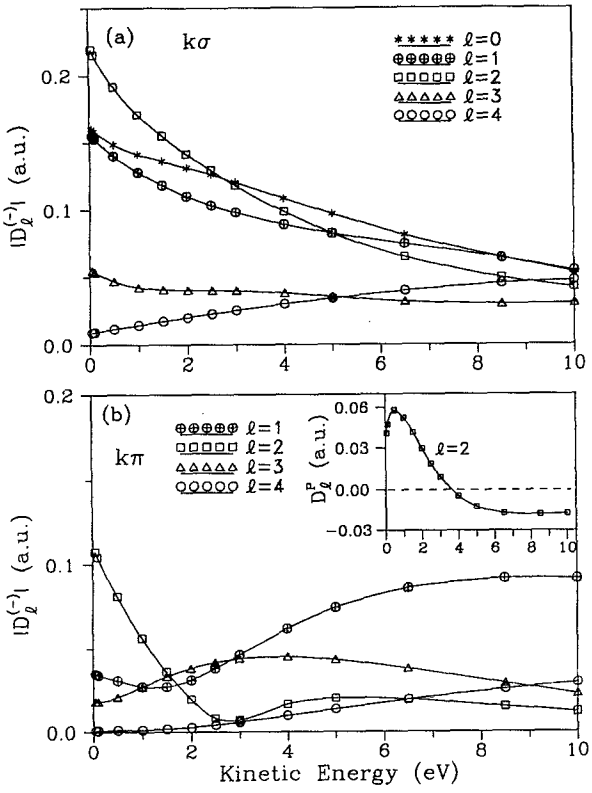

FIG. 1. Magnitude $|D_\ell^{(-)}|$ of the partial wave components of the photoelectron matrix element for photoionization of the $B\,^2\Sigma^+$ ($4s\sigma$) Rydberg state of SiF for the (a) $4s\sigma \rightarrow k\sigma$ and (b) $4s\sigma \rightarrow k\pi$ ionization channels. The inset shows the principal-value dipole amplitude D_ℓ^P for the $l=2$ component.

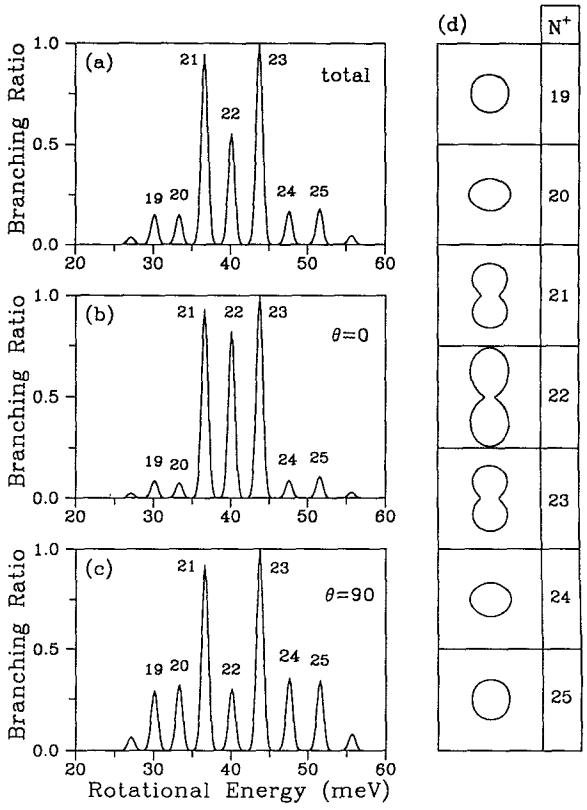

FIG. 2. Photoelectron spectra with laser tuned to the $R_{22}(21.5)$ line of the $X \rightarrow B$ transition for (a) the total cross section; (b) laser light polarized parallel ($\theta=0$); and (c) perpendicular ($\theta=90$) to photoelectron detection; and (d) the associated photoelectron angular distributions. $\theta=0$ is vertical in angular distributions. $\Delta N=0$ transition corresponds to $N^+=22$.

$=22$) state created by single-photon excitation is determined by a 3-j symbol of Eq. (3) with $n=1$ for this R_{22} rotational branch. The calculated spectra are convoluted with a Gaussian detection function having a full-width at half-maximum (FWHM) of 1 meV. We recognize that such spectral resolution can generally not be achieved in conventional photoelectron detection. However, we chose this resolution merely to illustrate the photoionization dynamics and compare with those for photoionization of NO.[6] Rotationally resolved spectra may be achieved by choosing rotational branches with higher J or using zero-kinetic-energy (ZEKE) detection and we believe the underlying dynamics will be similar. The photoelectron kinetic energy is about 1.43 eV. In addition to the expected $\Delta N=$even transitions, unusual $\Delta N=$odd (especially $\Delta N=\pm 1$) transitions are predicted. On the basis of the parity selection rule of Eq. (5) these odd ΔN transitions arise from even l contributions to the photoelectron matrix element. This behavior simply reflects the extraordinarily strong s and d waves in the electronic continua (see Fig. 1). Note that these unexpected $\Delta N=$odd transitions would be more evident in ZEKE measurements since the effect of the Cooper minimum in the d wave of the $k\pi$ continuum [Fig. 1(b)] should be less pronounced at threshold. On the other hand, strong $\Delta N=0$ and weaker $\Delta N=\pm 1, \pm 2$ transitions are observed for photoionization of the $A\,^2\Sigma^+$ ($3s\sigma$) state of NO (Refs. 6, 25, and 26). Comparison of the $|D_l^{(-)}|$'s for the $B\,^2\Sigma^+$ ($4s\sigma$) state of SiF (Fig. 1) and the $A\,^2\Sigma^+$ ($3s\sigma$) state of NO (see Fig. 2 of Ref. 7) reveals that the B state of SiF has much larger s and d wave and much weaker f wave contributions to its photoelectron matrix element. The odd partial wave components of the photoelectron matrix element ($|D_l^{(-)}|$) in the $k\pi$ channel also show minima near threshold. Examination of $|D_l^{(-)}|$ for the $B\,^2\Sigma^+$ ($4s\sigma$) state (Fig. 1) shows that these minima in the p and f components of $|D_l^{(-)}|$ in the $k\pi$ channel also play an important role in the occurrence of the $\Delta N=\pm 1$ peaks, since their depletion subsequently enhances the relative importance of the d ($l=2$) wave. Thus strong l mixing and the presence of minima in the electronic continuum are responsible for the occurrence of these unexpected $\Delta N=\pm 1, \pm 3$ peaks.

The photoelectron angular distributions of Fig. 2(d) clearly depend on the rotational level of the ion and reflect the angular momentum composition of the photoelectron orbitals. Also, according to the parity selection rule of Eq. (5), only even (odd) partial waves contribute to $\Delta N=$odd (even) transitions. To provide some insight into the underlying dynamics of these distributions, we give the magnitudes of the angular momentum components of the photoelectron matrix element at 1.5 eV. These are as follows:

This article is copyrighted as indicated in the article. Reuse of AIP content is subject to the terms at: http://scitation.aip.org/termsconditions. Downloaded to IP: 131.215.248.200 On: Sat, 17 Oct 2015 05:28:26

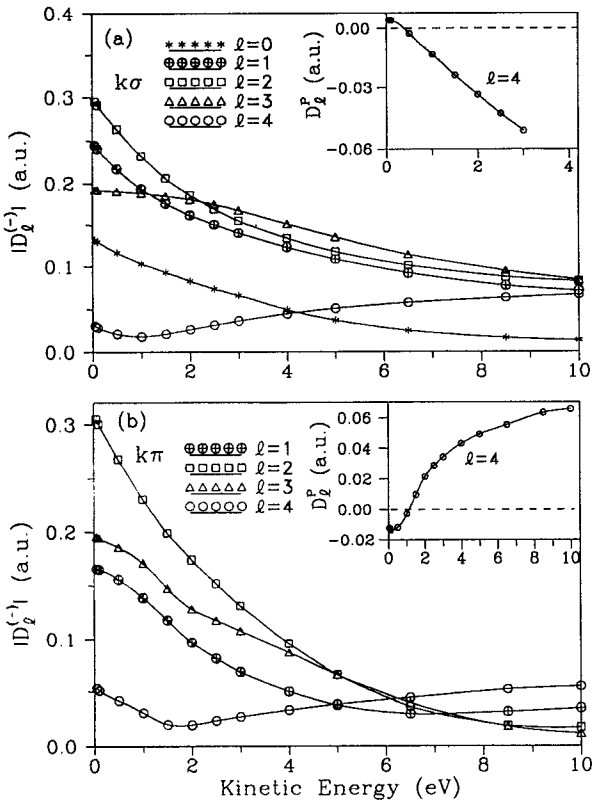

FIG. 3. Magnitude $|D_l^{(-)}|$ of the partial wave components of the photoelectron matrix element for photoionization of the $C''\,^2\Sigma^+$ $(4p\sigma)$ Rydberg state of SiF for the (a) $4p\sigma \rightarrow k\sigma$ and (b) $4p\sigma \rightarrow k\pi$ ionization channels. The inset shows the principal-value dipole amplitude D_l^P for the $l=4$ component.

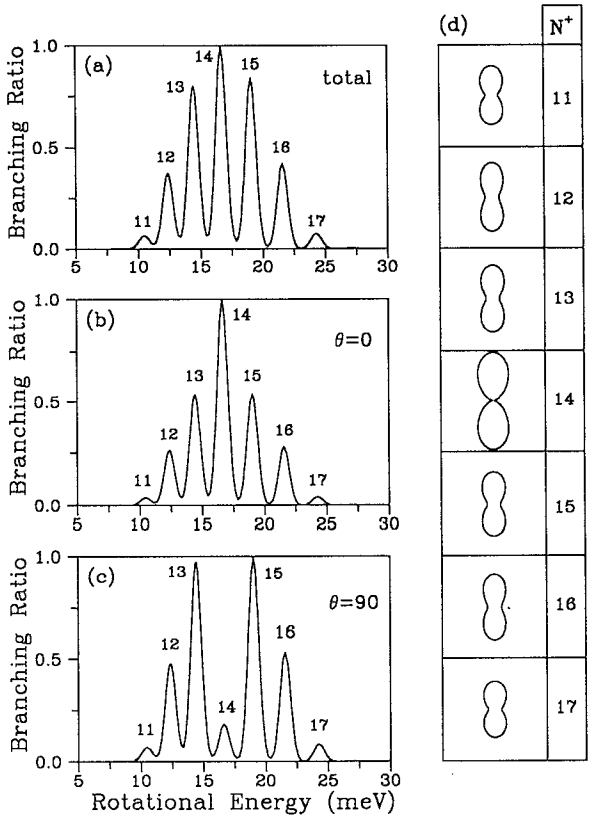

FIG. 4. The same as in Fig. 2 except for (2+1) REMPI via the $S_{21}(11.5)$ rotational branch of the $C''\,^2\Sigma^+$ state of SiF and $\Delta N=0$ transition corresponding to $N^+=14$.

0.1363, 0.1186, 0.1552, 0.0405, and 0.0173 for $l=0-4$, respectively, in the $k\sigma$ channel and 0.0273, 0.0361, 0.0334, and 0.0017 for $l=1-4$, respectively, in the $k\pi$ channel. Clearly, the $k\sigma$ channel contributes significantly to the photoionization dynamics.

B. (2+1) REMPI via the $C''\,^2\Sigma^+$ Rydberg state

Figure 3 shows the $|D_l^{(-)}|$'s for the $4p\sigma \rightarrow k\sigma$ [Fig. 3(a)] and $4p\sigma \rightarrow k\pi$ [Fig. 3(b)] photoionization channels of the $C''\,^2\Sigma^+$ $(4p\sigma)$ state. Strong p and f partial waves are predicted in addition to the dominant s and d waves expected in an atomiclike picture for photoionization of this $4p\sigma$ orbital. Since the $4p\sigma$ orbital only has about 16% s and 10% d character, these odd waves arise primarily from strong l mixing in the electronic continuum. Cooper minima are also predicted in the $l=4$ component of the $k\sigma$ and $k\pi$ photoionization channels. The corresponding sign changes in D_l^P are shown in the insets of Fig. 3. Cooper minima in the $l=4$ wave have not been reported before.

Figure 4 shows the photoelectron spectra [integrated cross sections in Fig. 4(a)] and with the laser polarized parallel [Fig. 4(b)] and perpendicular [Fig. 4(c)] to the flight direction of the photoelectron and the associated photoelectron angular distributions [Fig. 4(d)] resulting from (2+1) REMPI via the $S_{21}(11.5)$ rotational branch of the $C'\,^2\Sigma^+$ $(4p\sigma)$ Rydberg state of SiF. The photoelectron kinetic energy is about 0.87 eV. These photoelectron spectra are convoluted with a Gaussian detection function with an FWHM of 1 meV. The alignment of the $C''\,^2\Sigma^+$ $(v=0, N=14)$ state is determined from the 3-j symbol of Eq. (3) with $n=2$. Strong and unexpected $\Delta N=$even (especially $\Delta N=0$) transitions are predicted in addition to the expected $\Delta N=$odd transitions for photoionization of a $4p\sigma$ orbital. The $\Delta N=0$ peak, which is the most intense in Figs. 4(a) and 4(b), arises from the p and f angular momentum contributions to the photoelectron matrix element, in accordance with the parity selection rule of Eq. (5). Unexpected $\Delta N=0$ transitions were also observed in photoionization of the $D\,^2\Sigma^+$ $(3p\sigma)$ state of NO (Refs. 6 and 7), the $D\,^2\Sigma^-$ $(3p\sigma)$ state of OH (Ref. 27), and the $f\,^1\Pi$ $(3p\sigma)$ state of NH (Refs. 23 and 28), but these were seen to be due to the presence of the Cooper minima in the ionization channels. However, the $\Delta N=0$ peak for photoionization of the $C''\,^2\Sigma^+$ $(4p\sigma)$ state of SiF is predominantly due to strong l mixing in the electronic continuum and not to the weaker Cooper minima in the $l=4$ wave of the $k\sigma$ and $k\pi$ channels. Comparison of the photoelectron spectra of Fig. 4 with those for (2+1) REMPI via the $D\,^2\Sigma^+$ $(3p\sigma)$ state of NO (Refs. 6 and 7) shows that the $\Delta N=\pm 3$ transitions for the C'' state of SiF are much weaker. This difference is also reflected in the photoelectron angular distributions and can be accounted for by the

This article is copyrighted as indicated in the article. Reuse of AIP content is subject to the terms at: http://scitation.aip.org/termsconditions. Downloaded to IP: 131.215.248.200 On: Sat, 17 Oct 2015 05:28:26

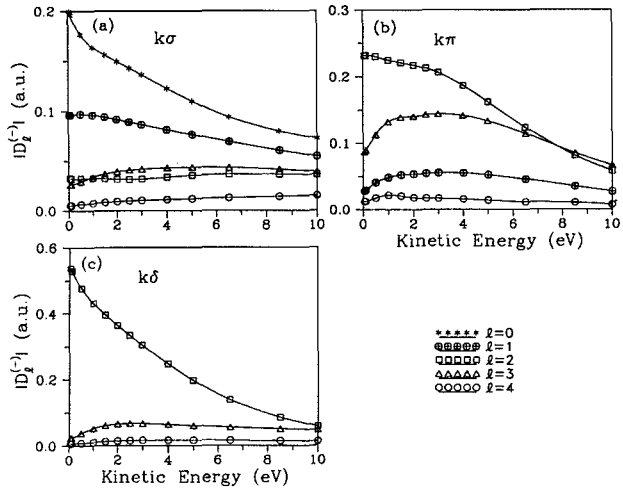

FIG. 5. Magnitude $|D_\ell^{(-)}|$ of the partial wave components of the photoelectron matrix element for photoionization of the $C'\,^2\Pi$ ($4p\pi$) Rydberg state of SiF for the (a) $4p\pi \rightarrow k\sigma$, (b) $4p\pi \rightarrow k\pi$, and (c) $4p\pi \rightarrow k\delta$ ionization channels.

angular momentum composition of the photoelectron matrix elements shown in Fig. 3.

C. (2+1) REMPI via the $C'\,^2\Pi$ Rydberg state

Figure 5 shows the $|D_\ell^{(-)}|$ elements for the $4p\pi \rightarrow k\sigma$ [Fig. 5(a)], $4p\pi \rightarrow k\pi$ [Fig. 5(b)], and $4p\pi \rightarrow k\delta$ [Fig. 5(c)] channels for photoionization of the $C'\,^2\Pi$ ($4p\pi$) state of SiF. In contrast to the $B\,^2\Sigma^+$ and $C''\,^2\Sigma^+$ states, no evidence of Cooper minima is seen within the kinetic energy range studied. The 4π orbital has nearly pure $4p$ (95%) character and hence it is more difficult to form a Cooper minimum since there are two nodes in the radial wave function. However, a Cooper minimum was seen in the $l=2$ wave of the $k\delta$ channel for photoionization of the $C\,^2\Pi$ ($3p\pi$) state of NO (Ref. 7).

Figures 6 and 7 show photoelectron spectra for (2+1) REMPI via the $Q_{21}(13.5)$ *ee* and *ff* rotational lines of the $X \rightarrow C'$ transition, respectively. The associated photoelectron angular distributions are also shown in Figs. 6 and 7. The alignment of the $C'\,^2\Pi$ ($v=0, J=13.5, N=14$) state via the *ee* and *ff* lines were determined from Eq. (4) by including eight $^2\Sigma^+$, seven $^2\Pi$, and two $^2\Delta$ virtual states (obtained from IVO calculations) and using the intermediate coupling scheme between Hund's cases (a) and (b) in evaluating the B_0 and B_2 factors of Eq. (4). Inclusion of more virtual states in the calculation of the alignment led to no significant changes in the rotationally resolved photoelectron spectra. The photoelectron energy is about 0.40 eV and the spectra are convoluted with a Gaussian detection function with an FWHM of 1 meV. Important features associated with Figs. 6 and 7 are (1) strong asymmetry in the spectral profiles (peak intensities) with respect to $\Delta N=0$ transition is predicted for both *ee* and *ff* lines; (2) observable $\Delta N=\pm 1$ peaks in the *ee* line and $\Delta N=0, \pm 2$ peaks in the *ff* line. The parity selection rule of Eq. (6) shows that these peaks arise from odd partial wave

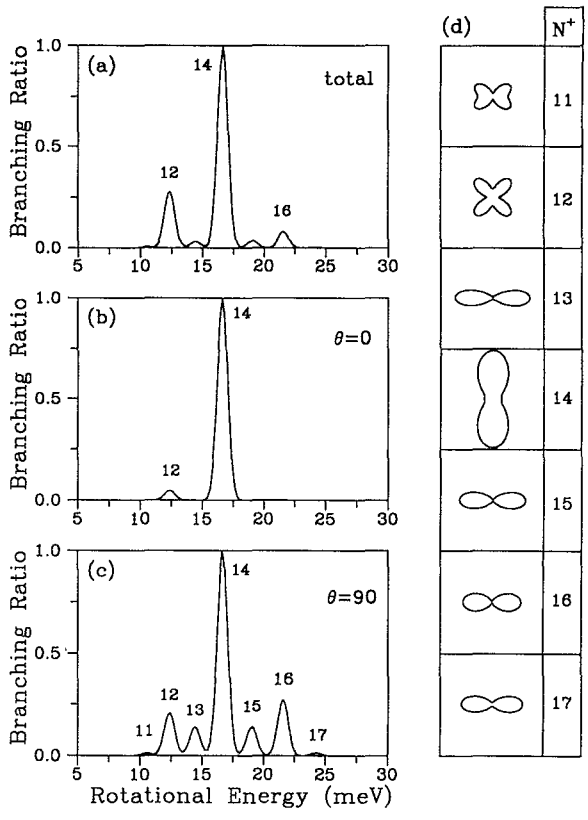

FIG. 6. The same as in Fig. 2 except for (2+1) REMPI via the $Q_{21}(13.5)$ *ee* rotational line of the $C'\,^2\Pi$ state of SiF and $\Delta N=0$ transition corresponding to $N^+=14$.

contributions to the photoelectron matrix element. These peaks are entirely molecular in origin since predominantly even partial waves would be expected in an atomiclike picture for photoionization of a $4p\pi$ orbital; (3) the $\Delta N=-2$ transition of the *ee* line and the $\Delta N=1$ of the *ff* line arise mainly from higher even partial wave contributions. This is evident from the photoelectron angular distributions; and (4) a $\Delta N=0, \pm 2$ propensity for the *ee* line and a $\Delta N=\pm 1$ propensity for the *ff* line, as expected for photoionization of a $4p\pi$ orbital. On the other hand, the photoelectron spectra via the $C\,^2\Pi$ ($3p\pi$) state of NO reveal no asymmetry in its spectra and no nonatomiclike transitions in a similar REMPI process.[7] Closer comparison of the $|D_\ell^{(-)}|$ for both systems shows stronger *p* and *f* waves and no Cooper minimum in the $C'\,^2\Pi$ state of SiF. These difference may be responsible for the asymmetrical behavior in the photoelectron spectra here.

Unlike the large Λ-doublet splitting in the $C\,^2\Pi$ state of NO, the separation between the $Q_{21}(13.5)$ *ee* and *ff* rotational lines for the $C'\,^2\Pi$ state of SiF is beyond the laser resolution. Figure 8 shows the calculated rotational branching ratios and associated photoelectron angular distributions resulting from (2+1) REMPI of SiF via the $Q_{21}(13.5)$ rotational branch assuming that the contributions from *ee* and *ff* rotational lines are not resolved. Again, asymmetrical spectra are seen with the most intense peak corresponding to $\Delta N=0$ ($N^+=14$). Each rotational

This article is copyrighted as indicated in the article. Reuse of AIP content is subject to the terms at: http://scitation.aip.org/termsconditions. Downloaded to IP: 131.215.248.200 On: Sat, 17 Oct 2015 05:28:26

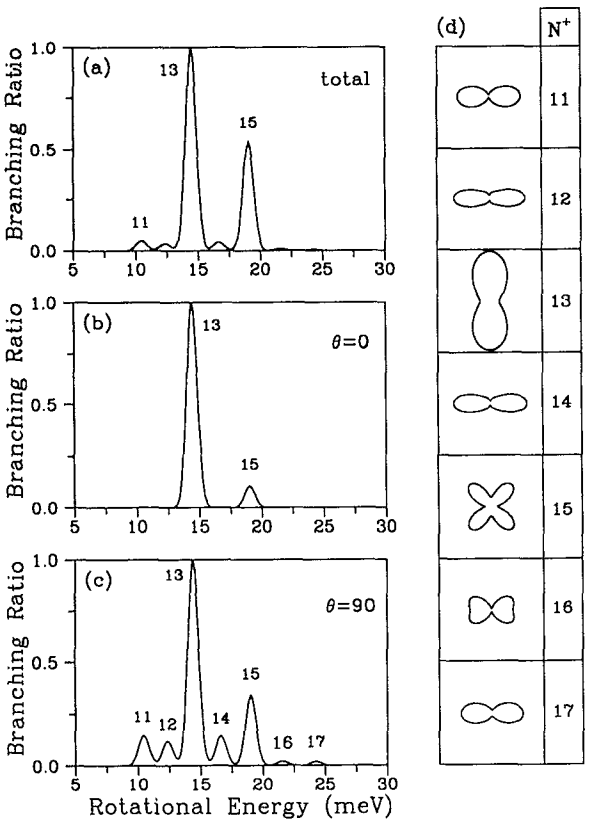

FIG. 7. The same as in Fig. 2 except for (2+1) REMPI via the $Q_{21}(13.5)$ *ff* rotational line of the $C'\,^2\Pi$ state of SiF and $\Delta N=0$ transition corresponding to $N^+=14$.

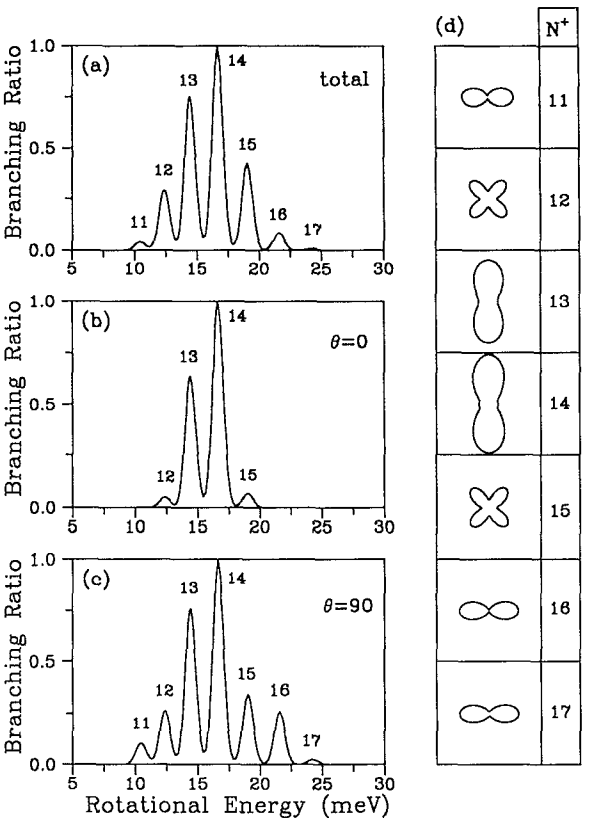

FIG. 8. The same as in Fig. 2 except for (2+1) REMPI via the $Q_{21}(13.5)$ *ee* and *ff* rotational lines of the $C'\,^2\Pi$ state of SiF and $\Delta N=0$ transition corresponding to $N^+=14$.

transition has contributions from both even and odd partial waves with stronger weights from even waves due to the almost pure p (95%) character of the $4p\pi$ orbital. The photoelectron angular distributions of Fig. 8(d) are obtained by incoherently summing the contributions from the *ee* and *ff* lines. Terms up to β_6 of Eq. (1) are included with $\beta_0=1$ and $\theta=0$ is vertical. The photoelectron angular distributions show significant contributions from higher partial waves.

ACKNOWLEDGMENTS

This work was supported by grants from the National Science Foundation, Air Force Office of Scientific Research, and the Office of Health and Environmental Research of the U.S. Department of Energy. We also acknowledge use of resources of the Jet Propulsion Laboratory/Caltech CRAY Y-MP2E/116 Supercomputer.

[1] H. F. Winters, J. Vacuum Sci. Technol. B **1**, 927 (1983).
[2] J. W. Coburn and H. F. Winters, Ann. Rev. Mat. Sci. **13**, 91 (1983).
[3] S. T. Pratt, P. M. Dehmer, and J. L. Dehmer, in *Advances in Multiphoton Processes and Spectroscopy*, edited by S. H. Lin (World Scientific, Singapore, 1988), and the references and tabulation of REMPI photoelectron spectroscopy studies therein.
[4] C. S. Dulcey and J. W. Hudgens, Chem. Phys. Lett. **118**, 444 (1985).
[5] J. A. Dagata, D. W. Squire, C. S. Dulcey, D. S. Y. Hsu, and M. C. Lin, Chem. Phys. Lett. **134**, 151 (1987).
[6] K. S. Viswanathan, E. Sekreta, E. R. Davidson, and J. P. Reilly, J. Phys. Chem. **90**, 5078 (1986).
[7] K. Wang, J. A. Stephens, and V. McKoy, J. Chem. Phys. **95**, 6456 (1991).
[8] J. B. Halpern, H. Zacharias, and R. Wallenstein, J. Mol. Spectrosc. **79**, 1 (1980).
[9] L. T. Earls, Phys. Rev. **48**, 423 (1935).
[10] M. Dubs, U. Brühlmann, and J. R. Huber, J. Chem. Phys. **84**, 3106 (1986).
[11] S. N. Dixit and V. McKoy, Chem. Phys. Lett. **128**, 49 (1986).
[12] J. M. Robbe, Y. Houbrechts, I. Dubois, and H. Bredohl, J. Mol. Spectrosc. **112**, 228 (1985).
[13] K. Wang and V. McKoy, J. Chem. Phys. **95**, 4977 (1991).
[14] J. Xie and R. N. Zare, J. Chem. Phys. **93**, 3033 (1990).
[15] G. Raseev and N. Cherepkov, Phys. Rev. A **42**, 3948 (1990).
[16] J. M. Brown, J. T. Hougen, K. P. Huber, J. W. C. Johns, I. Kopp, H. Lefebvre-Brion, A. J. Merer, D. A. Ramsay, J. Rostas, and R. N. Zare, J. Mol. Spectrosc. **55**, 500 (1975).
[17] W. J. Hunt and W. A. Goddard, Chem. Phys. Lett. **3**, 414 (1969).
[18] A. D. McLean and G. S. Chandler, J. Chem. Phys. **72**, 5639 (1980).
[19] T. H. Dunning, Jr., J. Chem. Phys. **55**, 716 (1971).
[20] R. R. Lucchese, G. Raseev, and V. McKoy, Phys. Rev. A **25**, 2572 (1982).
[21] R. R. Lucchese, K. Takatsuka, and V. McKoy, Phys. Rep. **131**, 147 (1986).
[22] J. A. Stephens and V. McKoy, J. Chem. Phys. **93**, 7863 (1990).
[23] K. Wang, J. A. Stephens, V. McKoy, E. de Beer, C. A. de Lange, and N. P. C. Westwood, J. Chem. Phys. **97**, 211 (1992).
[24] K. A. Peterson, R. C. Woods, P. Rosmus, and H.-J. Werner, J. Chem. Phys. **93**, 1889 (1990).

This article is copyrighted as indicated in the article. Reuse of AIP content is subject to the terms at: http://scitation.aip.org/termsconditions. Downloaded to IP: 131.215.248.200 On: Sat, 17 Oct 2015 05:28:26

[25] S. N. Dixit, D. L. Lynch, V. McKoy, and W. M. Huo, Phys. Rev. A **32**, 1267 (1985).
[26] S. W. Allendorf, D. J. Leahy, D. C. Jacobs, and R. N. Zare, J. Chem. Phys. **91**, 2216 (1989).
[27] E. de Beer, C. A. de Lange, J. A. Stephens, K. Wang, and V. McKoy, J. Chem. Phys. **95**, 714 (1991).
[28] E. de Beer, M. Born, C. A. de Lange, and N. P. C. Westwood, Chem. Phys. Lett. **186**, 40 (1991)

This article is copyrighted as indicated in the article. Reuse of AIP content is subject to the terms at: http://scitation.aip.org/termsconditions. Downloaded to IP: 131.215.248.200 On: Sat, 17 Oct 2015 05:28:26